THE JOURNAL OF PHYSICAL CHEMISTRY Letters

Letter

pubs.acs.org/JPCL

Deformed Surface Oxides: Uncommon Structure of a (6 × 1) NiO Surface Oxide on Rh(111)

T. Franz,[†] J. Zabloudil,[†] F. Mittendorfer,*[,†,‡] L. Gragnaniello,[§] G. Parteder,[§] F. Allegretti,[§,⊥] S. Surnev,[§] and F.P. Netzer[§]

[†]Faculty of Physics, Vienna University and Center for Computational Materials Science, A-1090 Wien, Austria

[‡]Instiute of Applied Physics, and Center for Computational Materials Science, TU Vienna, Austria

[§]Institute of Physics, Surface and Interface Physics, Karl-Franzens University Graz, A-8010 Graz, Austria

ABSTRACT: We have investigated the formation of a nickel oxide monolayer on Rh(111) by scanning tunneling microscopy (STM), high-resolution electron energy loss spectroscopy (HREELS), and density functional theory (DFT) calculations. This monolayer displays a corrugated (6 × 1) superstructure, with a formal Ni_5O_5 stoichiometry. The interplay between polarity and interface energy leads to the formation of a structure with pronounced troughs, which may be regarded as a building deformation, containing building blocks derived from nonpolar (100) and polar (111) NiO surface terminations. The calculations also show that the (6 × 1) Ni_5O_5 phase has a higher thermodynamic stability than the related octopolar NiO bulk terminations.

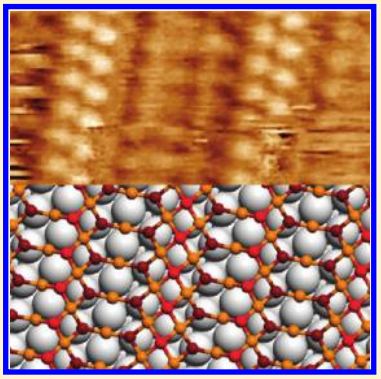

SECTION: Surfaces, Interfaces, Catalysis

In recent years, the surface and interface properties of 3d oxide materials have received considerable interest due to their wide range of technological applications, ranging from magnetic storage media to catalytic materials.[1,2] Yet, even the structure of an oxide surface, such as NiO, can be rather complex. Due to the rocksalt (NaCl) bulk structure of nickel oxide, the crystal can display both nonpolar surfaces such as NiO(100), with no macroscopic dipole moment, and also polar surfaces such as NiO(111). In the case of a polar surface, the resulting polar instability has to be compensated for by either structural or electronic modifications. An overview of the dominant compensating mechanisms can be found in a recent review by Goniakowsky.[3] In the case of the polar NiO(111) surface, surface X-ray diffraction experiments[4,5] indicate a compensation by the formation of a p(2 × 2) octopolar reconstruction.

On the other hand, if the oxide surface is not the termination of the NiO bulk structure but is present as an ultrathin layer (with a thickness of only a few nanometers) supported on a single-crystal metal substrate, the structural and electronic flexibility at the interface allows for the presence of new phases that would be unstable in the thick-film limit. Moreover, such surface oxide structures are determined not only by polarity considerations but also by the strain induced by the lattice mismatch between the metallic substrate material and the (bulk) nickel oxide. In particular, fcc (111) surfaces offer an interesting playground as the lattice symmetry of the substrate favors a polar (111) termination while the polarity considerations usually predict a lower surface energy for the nonpolar (100) bulk terminations. In addition, low dimensionality aspects of the supported Ni oxide structures have to be considered and may give rise to different physical behavior.[6,7] Ni oxide films with a thickness of several atomic layers have been investigated with scanning tunneling microscopy (STM) and X-ray photon spectroscopy (XPS) on Ni(111),[8,9] Cu(111),[10] and Au(111).[11] Yet, the knowledge about the structural properties at the onset of the growth of the NiO layers is rather sparse.

In this Letter, we report on the formation of a (6 × 1) NiO monolayer supported on a Rh(111) single-crystal surface and analyze the influence of the polarity and strain on the structure of this surface oxide phase. Oxidation of submonolayer Ni films in 5 × 10^{-8} mbar of oxygen causes the formation of two-dimensional (2-D) islands exhibiting a (6 × 1) structure (Figure 1a), which grow in size with increasing Ni coverage and eventually form a wetting layer at 1 ML (Figure 1b). The atomically resolved STM image in Figure 1c shows that the (6 × 1) structure displays zigzag ridges aligned pseudomorphically along the ⟨110⟩ substrate directions, which are separated by 6 Rh lattice constants, yielding the (6 × 1) periodicity (the unit cell is indicated on the image). Between the ridges, hexagonally ordered areas are visible. The atomic corrugations along and across the ridges are 0.1 and 0.3 Å, respectively. Occasionally, other ridge periodicities like (4 × 1) and (2 × 1) have been also

Received: November 18, 2011
Accepted: December 27, 2011
Published: December 27, 2011

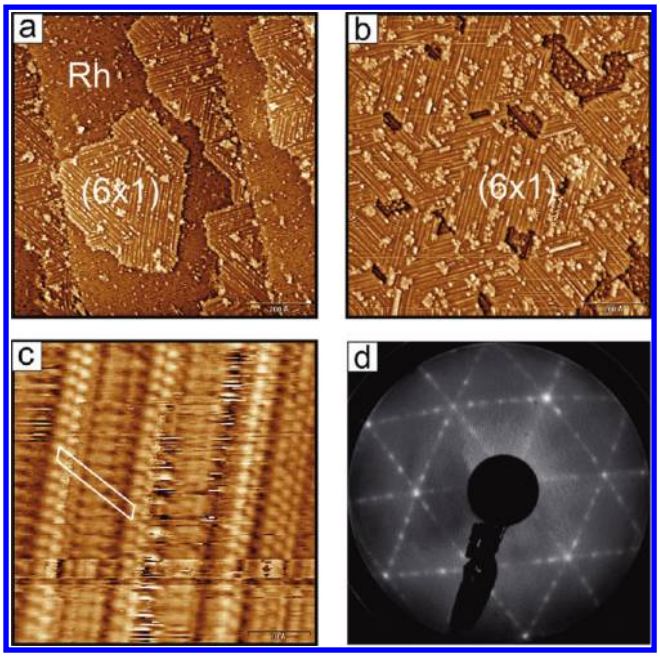

Figure 1. Large-scale (1000 Å × 1000 Å, +1.0 V, 0.2 nA) STM images of the (6 × 1) structure of Ni oxide on Rh(111) at a coverage of (a) 0.5 and (b) 1 ML; (c) high-resolution STM image (50 Å × 50 Å, +8 mV, 1.5 nA) revealing details of the (6 × 1) structure; (d) LEED image (E_p = 150 eV).

observed in STM, but the (6 × 1) is the dominant structure of the large scale, as confirmed by the LEED pattern, shown in Figure 1d. 2-D Ni oxide structures with a (6 × 1) and (2 × 1) periodicity have been also observed previously on a stepped Rh(15 15 13) surface in the monolayer coverage range,[12] but no structural models have been proposed yet. Ni oxide layers with a (7 × 1) structure, grown on a Pt(111) surface under similar preparation conditions,[13] show a very similar appearance in the STM images as the (6 × 1) phase. This structural similarity indicates that the (6 × 1) Ni oxide phase is not specific for a given oxide−metal interface but rather derives its stability from polarity cancellation and/or low surface energy effects, as discussed below.

Extensive DFT simulations using genetic algorithms and simulated annealing approaches allow us to determine the structure (Figure 2) and predict the stability of the (6 × 1) Ni oxide phase. The calculations show that the energetically favored structure is a Ni_5O_5 layer in a (6 × 1) Rh supercell at the chemical potential corresponding to the experimental conditions (μ_O = −1.25 eV). A model of this structure is presented in Figure 2a,b. Although the structure consists formally of a single NiO monolayer with a Ni_5O_5 stoichiometry, it displays a sizable corrugation of 1.2 Å. The simulated STM images (Figure 2c,d) display bright stripes, separated by (electronically) lower regions, in good agreement with the experimental data. Although the deep minima in the simulations are less pronounced in the experimental images, we attribute this difference to smearing and convolution effects originating from the final size of the STM tip.

At closer look, two types of building blocks can be identified at the surface, one triangular unit with a three-fold-coordinated oxygen atom and a rectangular building block with a four-fold-coordinated oxygen. Both elements are closely related to selected surface orientations of the NiO (rocksalt) bulk crystal, corresponding either to the (100) orientation (four-fold O) or

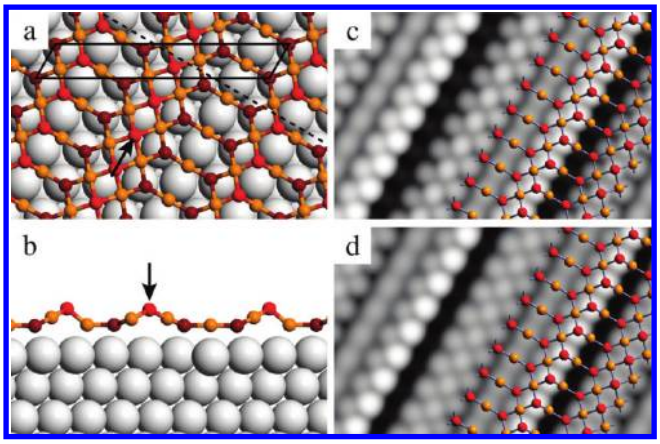

Figure 2. (a) Top view and (b) side view of the structural model for the (6 × 1) Ni_5O_5 structure. Ni (Rh) atoms are shown in orange (white), lower O atoms are in dark red, and higher O atoms are in bright red. The cutting plane for (b) is indicated as a black dashed line in (a). Simulation of the STM images (±0.2 eV) for the (c) occupied and (d) unoccupied states.

to the (111) orientation (three-fold O), respectively. Indeed, flat monolayers corresponding to these two orientations have been observed for related surface oxides, such as CoO/Pd(100)[14] or RhO_2/Rh(111).[15] The structure of the full oxide layer shows a clear correlation between the local building block and the interaction with the Rh(111) substrate. On the one hand, the three lower-lying oxygen atoms (Figure 2b) are positioned on top of the substrate Rh atoms [d(O−Rh) = 2.10 Å] and thus anchor the NiO layer to the Rh surface. On the other hand, the two higher O atoms display a certain flexibility to connect the network and appear in both triangular and rectangular units. It should be noted that with a Ni−Ni distance of 2.70 Å along the Rh rows and 2.50 Å in the perpendicular direction, the arrangement of the Ni atoms in the rectangular units is strongly compressed with respect to the ideal NiO(100) bulk planes (2.96 Å), resulting in a local deformation of the layer with a uniaxial buckling (Figure 2a,b, black arrows).

The HREELS spectra (Figure 3) provide additional information on the chemical composition and structure of the (6 × 1) NiO oxide phase and allow us to confirm the predicted model. The (6 × 1) phase at 1 ML exhibits a phonon loss structure (Figure 3a) consisting of a main loss peak at 60.5 meV, which is asymmetrically broadened at the high-energy side, and a second peak at 51 meV. Indeed, this observation is in very good agreement with the calculated vibrational spectrum of the Ni_5O_5 (6 × 1) model (Figure 3b), which shows two dipole active modes for the out-of-plane vibrations of the uppermost O atoms (Figure 2, bright red atoms) at 63 and 54 meV. For comparison, thicker (Θ > 3 ML) Ni oxide films on Rh(111) exhibit different phonon losses at 68 and 54 meV, which are characteristic of bulk NiO crystals.[16]

Why do we observe a high stability for this rather complex structure? A comparison of the thermodynamic stability of various competing phases (Figure 4) shows that the sizable lattice mismatch between the Rh substrate (lattice parameter a = 3.80 Å) and both the metallic Ni (a = 3.52 Å) and the bulk NiO lattices (a = 4.19 Å) plays a key role as it hinders an epitaxial growth of the corresponding films. The phase diagram shows clearly that the epitaxially grown Ni films are highly strained and thus rather unstable (Figure 4, orange dashed line). Even though the adsorption of p(2 × 1) oxygen leads to a

dx.doi.org/10.1021/jz201527z | J. Phys. Chem.Lett. 2012, 3, 186−190

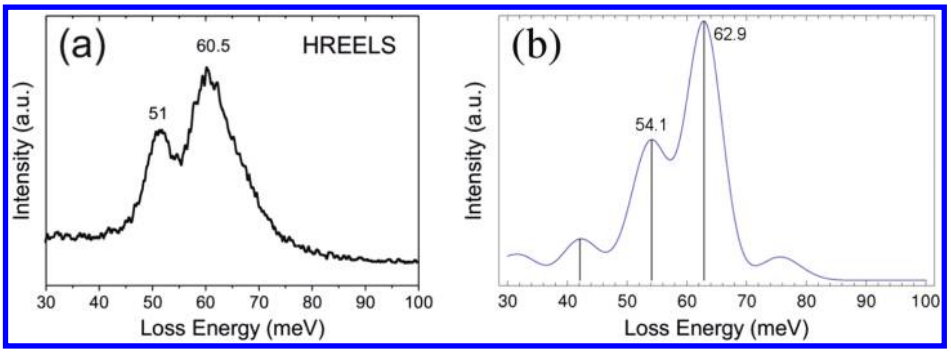

Figure 3. (a) Experimental HREELS spectrum of the (6 × 1) NiO layer on Rh(111) and (b) the calculated vibrational spectrum weighted by the dipole activity of the modes.

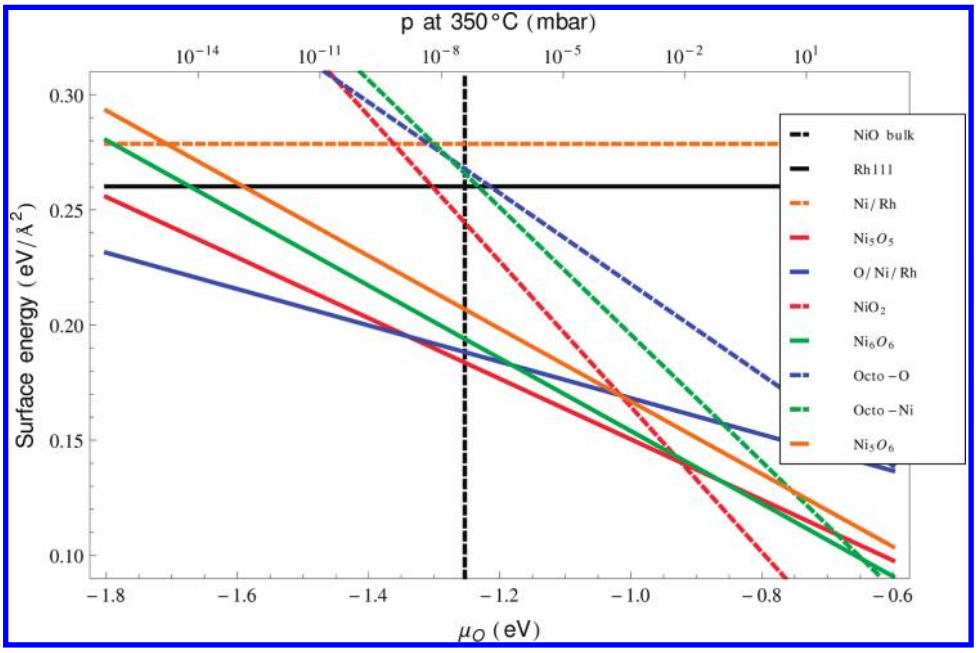

Figure 4. Phase stability diagram of monolayer-thick NiO layers on Rh(111).

reduction of the stress of the Ni layer (Figure 4, blue line), a mere oxygen adsorption phase (see the model in Figure 5b) remains only thermodynamically stable under oxygen-poor conditions (μ(O) < −1.3 eV). This latter structure may thus correspond to the p(2 × 1) minority phase, observed to coexist with the (6 × 1) majority phase in the experiment, which marks the onset of the oxidation of the Ni layer. It should be noted that the high surface stress prevents the formation of a p(2 × 1) phase on the *bare* Ni(111) surface,[17] but for the supported Ni monolayer, a certain amount of oxygen is even needed for a sufficient expansion of the NiO layer.

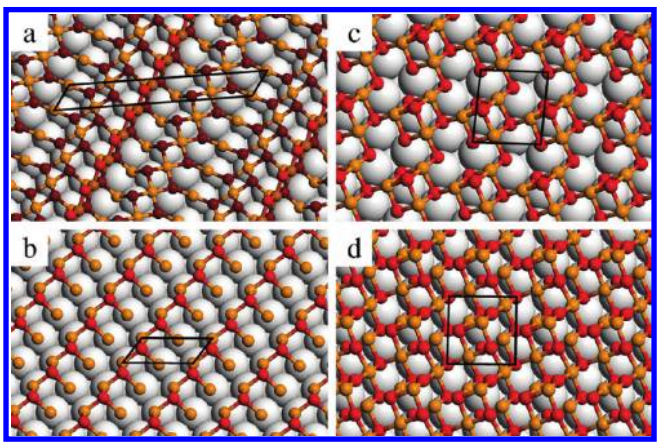

Figure 5. Structural models for (a) (6 × 1) Ni_6O_6, (b) p(2 × 1) chemisorbed O on Ni/Rh(111), and (c) O-terminated and (d) Ni-terminated octopolar reconstructions. Rh atoms are depicted in white, O atoms in red, and Ni atoms in orange.

The (6 × 1) Ni_5O_5 stoichiometry (Figure 4, red line) represents already the highest oxygen content that can be accommodated in a single flat NiO layer as additional oxygen can only be incorporated in the surface oxide layer by increasing both the Ni and O coverage. Figure 5a displays the optimized (hypothetical) Ni_6O_6 structure with a (6 × 1) cell, which can be seen as the onset for the growth of an additional layer. Evidently, the structure is closely related to the Ni_5O_5 model but with an additional Ni atom in the rectangular unit of the NiO film marking the growth of the second layer. Nevertheless, the phase diagram clearly displays that this precursor structure is only metastable, even though the energy difference to the Ni_5O_5 structure is rather small. Evaluating the related work functions allows one to assess the role of the induced surface dipoles. The calculations show a pronounced effect of the electronic contributions. While the calculated work

dx.doi.org/10.1021/jz201527z | J. Phys. Chem.Lett. 2012, 3, 186–190

function of the bare Rh(111) surface is increased from ϕ = 5.13 eV to a value of 5.96 eV ($\Delta\phi$ = 0.8 eV), the work function after the formation of the Ni_5O_5 layer is only increased to 5.17 eV ($\Delta\phi$ = 0.03 eV). On the contrary, the presence of a Ni_6O_6 layer would lead to change in the work function of $\Delta\phi$ = 1.37 eV. Therefore, only a very minor surface dipole is induced by the formation of the Ni_5O_5 layer.

If the oxygen content is increased even further, a thicker NiO film is formed. A comparison of several terminations demonstrates that the ultrathin film with a thickness slightly larger than 1 ML does not correspond to either oxygen- (Figure 4, blue dashed line, model in Figure 5c) or Ni-terminated octopolar reconstructions (Figure 4, green dashed line, model in Figure 5d), which have been observed for the bulk NiO(111) surface.[4,5] Instead, we predict that the NiO layer is transformed into an epitaxial (nonpolar) NiO_2 trilayer in an oxygen-rich environment. Yet, also the transformation into this high-coverage structure is only predicted for a significantly higher chemical potential of >−1.0 eV, which corresponds to rather high oxygen partial pressures (Figure 4).

To conclude, a nonpolar (6 × 1) NiO film has been identified on the Rh(111) surface by STM and DFT calculations. The calculations demonstrate that the film has a formal stoichiometry of Ni_5O_5, which is the highest amount of oxygen that can be accommodated in a single NiO layer on this surface orientation. Due to the large lattice mismatch between the NiO oxide and the Rh(111) support, the Ni_5O_5 layer is not formed as a uniform structural film but consists of two different building blocks that are related to (111) and (100) NiO surface terminations. The combination of both structural elements leads to the formation of pronounced troughs along the [110] direction. These troughs create a potential template for the growth of low-dimensional nanostructures with a well-defined width.

EXPERIMENTAL AND THEORETICAL DETAILS

Nickel oxide layers with a thickness of up to 1 monolayer (one monolayer (ML) is defined by the number of surface atoms on the Rh(111) surface) were prepared by UHV deposition of Ni metal onto a clean Rh(111) surface held at 150 °C, followed by oxidation in a molecular oxygen atmosphere (postoxidation). The sample temperature during the oxidation was kept at 350 °C for 5 min, and the oxygen pressure was 5×10^{-8} mbar. The Ni deposition rate was controlled by a quartz microbalance. The STM experiments were performed in a custom-designed variable-temperature STM system, as described previously.[18] All STM images presented here have been recorded at room temperature and in constant-current mode. High-resolution electron energy loss spectroscopy (HREELS) measurements have been performed in a second UHV system[19] with a primary energy of 6.5 eV, in a specular reflection geometry of $\Theta_{in} = \Theta_{out}$ = 60°, with a typical resolution of 5 meV as measured at the full width at half-maximum (fwhm) of the reflected primary peak. Low-energy electron diffraction (LEED) has been used to control the structure of the nickel oxide films and thus to ensure identical oxide preparation conditions in both UHV chambers.

The spin-polarized calculations have been performed with the Vienna Ab-initio Simulatiuons Package (VASP),[20,21] using PAW potentials[22] and the PBE exchange−correlation functional.[23] The Brillouin zone integration was performed using a 24 × 24 × 1 *k*-point mesh for the primitive (1 × 1) cell. The Rh surface was modeled with a six-layer slab, allowing for relaxation of the uppermost three layers. The initial candidates for the NiO surface oxides were derived from simulations using genetic algorithms[24] and simulated annealing.[25] The respective surface stabilities have been evaluated in the ab initio thermodynamics framework, where the chemical potential of Ni is set to the Ni bulk binding energy of −5.47 eV and the chemical potential of O is referenced to the binding energy of −5.03 eV of the O_2 molecule. The STM simulations were performed in a Tersoff−Hamann approach for the charge distribution between the Fermi energy and ±0.2 eV.

AUTHOR INFORMATION

Present Address

[⊥]Physik Department E20, Technische Universität München, James-Franck Strasse, 85748 Garching, Germany.

ACKNOWLEDGMENTS

This work has been supported by the Austrian Science Funds (FWF) under Grant Numbers Y218, the SFB FOXSI (F4511-N16), and the ERC Advanced Grant SEPON. The Vienna Scientific Cluster (VSC) is acknowledged for computing time.

REFERENCES

(1) Knudsen, J.; Merte, L. R.; Peng, G.; Vang, R. T.; Resta, A.; Lægsgaard, E.; Andersen, J. N.; Mavrikakis, M.; Besenbacher, F. Low-Temperature CO Oxidation on Ni(111) and on a Au/Ni(111) Surface Alloy. *ACS Nano* **2010**, *4*, 4380.

(2) Peng, G.; Merte, L. R.; Vang, R. T.; Lægsgaard, E.; Besenbacher, F.; Mavrikakis, M. On the Mechanism of Low-Temperature CO Oxidation on Ni(111) and NiO(111) Surfaces. *J. Phys. Chem. C* **2010**, *114*, 21579.

(3) Goniakowsky, J.; Finocchi, F.; Noguera, C. Polarity of Oxide Surface and Nanostructures. *Rep. Prog. Phys.* **2008**, *71*, 016501.

(4) Barbier, A.; Mocuta, C.; Kuhlenbeck, H.; Peters, K. F.; Richter, B.; Renaud, G. Atomic Structure of the Polar NiO(111)-p(2 × 2) Surface. *Phys. Rev. Lett.* **2000**, *84*, 2897.

(5) Barbier, A.; Mocuta, C.; Neubeck, W.; Mulazzi, M.; Yakhou, F.; Chesnei, K.; Sollier, A.; Vettier, C.; de Bergevin, F. Surface and Bulk Spin Ordering of Antiferromagnetic Materials: NiO(111). *Phys. Rev. Lett.* **2004**, *93*, 257208.

(6) Schoiswohl, J.; Mittendorfer, F.; Surnev, S.; Ramsey, M. G.; Andersen, J. N.; Netzer, F. P. Chemical Reactivity of Ni−Rh Nanowires. *Phys. Rev. Lett.* **2006**, *97*, 126102.

(7) Surnev, S.; Allegretti, F.; Parteder, G.; Franz, T.; Mittendorfer, F.; Andersen, J. N.; Netzer, F. P. One-Dimensional Oxide−Metal Hybrid Structures: Site-Specific Enhanced Reactivity for CO Oxidation. *ChemPhysChem* **2010**, *11*, 2506.

(8) Kitakatsu, N.; Maurice, V.; Hinnen, C.; Marcus, P. Surface Hydroxylation and Local Structure of NiO Thin Films Formed on Ni(111). *Surf. Sci.* **1998**, *407*, 36.

(9) Yeo, B. S.; Chen, Z. H.; Sim, W. S. Efficient growth of Ordered Thin Oxide Films on Ni(111) by NiO_2 Oxidation. *Surf. Sci.* **2004**, *557*, 201.

(10) Stanescu, S.; Boeglin, C.; Barbier, A.; Deville, J.-P. Epitaxial Growth of Ultra-Thin NiO Films on Cu(111). *Surf. Sci.* **2004**, *549*, 172.

(11) Ventrice, C. A.; Bertrams, Th.; Hanneman, H.; Brodde, A.; Neddermeyer, H. Stable Reconstruction of the Polar (111) Surface of NiO on Au(111). *Phys. Rev. B* **1994**, *49*, 5773.

(12) Parteder, G.; Allegretti, F.; Wagner, M.; Ramsey, M. G.; Surnev, S.; Netzer, F. P. Growth and Oxidation of Ni Nanostructures on Stepped Rh surfaces. *J. Phys. Chem. C* **2008**, *112*, 19272.

(13) Hagendorf, Ch.; Shantyr, R.; Neddermeyer, H.; Widdra, W. Pressure Dependent NiO phase transitions and Ni Oxide Formation on Pt(111): An In Situ STM Study at Elevated Temperatures. *Phys. Chem. Chem. Phys.* **2006**, *8*, 1575.

(14) Gragnaniello, L.; Barcaro, G.; Sementa, L.; Allegretti, F.; Parteder, G.; Surnev, S.; Steurer, W.; Fortunelli, A.; Netzer, F. P. The Two-Dimensional Cobalt Oxide (9 × 2) Phase on Pd(100). *J. Chem. Phys.* **2011**, *134*, 184706.
(15) Mittendorfer, F. Low-Dimensional Surface Oxides in the Oxidation of Rh Particles. *J. Phys.: Condens. Matter* **2010**, *22*, 393001.
(16) Cox, P. A.; Williams, A. A. The Observation of Surface Optical Phonons and Low-Energy Electronic Transitions in NiO Single Crystals by Electron Energy Loss Spectroscopy. *Surf. Sci.* **1985**, *152/153*, 791.
(17) Kortan, A. R.; Park, R. L. Phase Diagram of Oxygen Chemisorbed on Ni(111). *Phys. Rev. B* **1981**, *23*, 6340.
(18) Surnev, S.; Vitali, L.; Ramsey, M. G.; Netzer, F. P.; Kresse, G.; Hafner, J. Growth and Structure of Ultrathin Vanadium Oxide Layers on Pd(111). *Phys. Rev. B* **2000**, *61*, 13945.
(19) Kardinal, I.; Ramsey, M. G.; Netzer, F. P. A Multiplicity of CN Bonding Configurations on Ni(110). *Surf. Sci.* **1997**, *376*, 229.
(20) Kresse, G.; Hafner, J. Ab Initio Molecular Dynamics for Liquid Metals. *Phys. Rev. B* **1993**, *47*, 558.
(21) Kresse, G.; Furthmüller, J. Efficiency of Ab-initio Total Energy Calculations for Metals and Semiconductors Using a Plane-Wave Basis Set. *J. Comput. Mater. Sci.* **1996**, *6*, 15.
(22) Kresse, G.; Joubert, D. From Ultrasoft Pseudopotentials tot he Projector Augmented-Wave Method. *Phys. Rev. B* **1999**, *59*, 1758.
(23) Perdew, J. P.; Burke, K.; Ernzerhof, M. Generalized Gradient Appoximation Made Simple. *Phys. Rev. Lett.* **1996**, *77*, 3865.
(24) Seriani, N.; Mittendorfer, F.; Kresse, G. Carbon in Palladium Catalysts: A Metastable Carbide. *J. Chem. Phys.* **2010**, *132*, 024711.
(25) Kresse, G.; Bergermayer, W.; Podloucky, R.; Lundgren, E.; Koller, R.; Schmid, M.; Varga, P. Complex Surface Reconstructions Solved by Ab Initio Molecular Dynamics. *Appl. Phys. A: Mater. Sci. Process.* **2003**, *76*, 701.